Available online at www.sciencedirect.com
SCIENCE DIRECT®
Journal of Power Sources 135 (2004) 110–121
JOURNAL OF POWER SOURCES
www.elsevier.com/locate/jpowsour

The effect of stoichiometry on dynamic behavior of a proton exchange membrane fuel cell (PEMFC) during load change

Sunhoe Kim, S. Shimpalee, J.W. Van Zee*

Department of Chemical Engineering, University of South Carolina, Columbia, SC 29208, USA

Received 24 February 2004; accepted 20 March 2004

Available online 25 June 2004

Abstract

Data are presented to show the transient response of a proton exchange membrane fuel cell (PEMFC) subjected to change in the load. Overshoot and undershoot behaviors of the steady-state current density were observed for various rates of change in the voltage during constant inlet flow rate conditions. The results of these experiments with a 25 cm^2 triple serpentine flow field indicate a correlation of the overshoot/undershoot behavior with initial and final stoichiometry. This transient analysis is potentially attractive in the operation of vehicle and stationary application and flow field designs.

Keywords: PEM; Fuel cells; Membrane electrode assembly; Electric vehicle; Transient; Stoichiometry; Electric load

1. Introduction

The control, design, and optimum operation of PEMFCs will require an understanding of its transient behavior when the current, voltage, or power changes. These dynamics would be important for residential and automotive applications and the transient operation may be a result of a sudden demand as an appliance starts or as a vehicle is accelerated or decelerated. These transients may be of sufficient amplitude and speed that fuel flow rates cannot be adjusted by feedback control and thus electrical capacitors are often used to stabilize the system output. Here we present experimental data to help understand how the fuel cell by default or design can act as a capacitor during the power demand surges.

While most of the studies of PEMFCs have focused on steady-state behavior, a few authors have considered transient operation of stacks [1–5]. For example, Hamelin et al. [1] demonstrated three different transients in their work on with a Ballard fuel cell stack model MK5-E, which has a total of 35 cells, of 10 kW maximum power, connected in series with a cell surface area of 232 cm^2. The first transient was a continuous load change with various amplitudes by changing the power in a square wave. The second was a higher frequency transient at very short times. In this part they replaced the back-pressure valve with a metering valve to maintain a fixed outlet flow, while the inlet mass flow controller was completely open to reduce the transient phenomena to the load alone. Finally, they studied DC + AC load communication and the noise from the AC/DC converter in the system. They emphasized the importance of studying transient behavior of fuel cell to understand how the fuel cell stack will behave under extreme conditions, for example, in case of current or voltage exceed certain limits.

Amphlett et al. [2] presented an analysis of a hybrid PEMFC/battery system with a system scaled down from a 400 kW fuel cell stack and 224 cell lead-acid battery suitable for submarine systems. They showed how their hybrid system and components interacted during charging or discharging. Those experiments followed a presentation of the dynamics during start-up, current change, and shut down of a Ballard Mark V 35-Cell 5 kW PEMFC stack where they compared the observed voltage response from a current change to their empirical model [3]. Emonts et al. [4] studied the dynamics of a PEMFC, a compact methanol reformer, and the choice of a short-term storage system for an automotive application. Kötz et al. [5] discussed the combinations of a PEMFC and supercapacitors for automotive applications. These experimental studies [1–5] were conducted under excess initial fuel and oxidant conditions and the load changes were not large enough to study starved fuel conditions.

* Corresponding author. Tel.: +1-803-777-2285; fax: +1-803-777-8028.
E-mail address: vanzee@engr.sc.edu (J.W. Van Zee).

0378-7753/$ – see front matter © 2004 Elsevier B.V. All rights reserved.
doi:10.1016/j.jpowsour.2004.03.060

Nomenclature

i	current density (A/cm^2)
K	steady-state gain (A/cm^2 V)
t	time (s)
V	cell voltage (V)
ΔV	cell voltage difference (V)

Greek letters

β	lead time constant (s)
δ	time constant for cell voltage (s)
ξ	damping coefficient
ρ	lead-to-lag ratio ($\rho = \beta/\tau$)
τ	Time constant (s)

In an effort to understand the dynamics of a PEMFC, we present data for a single cell with fixed flow rates. The transient operation is forced by rapid changes to the voltages and this allows observation of changes in the current and stoichiometry of the cell as discussed below. We are motivated by our recent three-dimensional numerical simulations for the transient response of fuel cell [6,7] in which we observed an overshoot in the current density when the voltage was changed at 1.0 V/s. The dynamics one-dimensional semi-empirical model of Ceraolo et al. [8] also leads discussions of when voltage overshoot observed in [3] may occur. Thus we designed experiments here to expand an understanding of this behavior.

2. Experimental

The objective of this work is to study the transient current response when the cell voltage is changed at a rate of approximately 0.2 V/s at fixed feed flow rates. These fixed flow rates result in the cell being exposed to different stoichiometries as the current changes as shown in Table 1. That is, here we present data for the response of the current when the cell voltage was changed from 0.7 to 0.5 V and from 0.5 to 0.7 V.

Four cases can be described as changes in operating conditions, such that the fuel and air are "normal", "starved", or "excess" (see Table 1). For example, Case 1a corresponds to the flow rates of 249 and 1040 cm^3/min at standard conditions[1] for the anode and cathode, respectively. These flow rates yield a stoichiometric change from 2.9/4.8 at $t \leq 0$ to 1.2/2.0 at $t = \infty$ for a current density of 0.62 A/cm^2 at 0.7 V and 1.48 A/cm^2 at 0.5 V. Thus Case 1a corresponds to a change in operation from a "excess" to a "normal" stoichiometry. Case 2a uses the same flow rates but we began the experiment at 0.5 V and increased the cell voltage to 0.7 V (i.e. 0.62 A/cm^2). Case 2a corresponds to a change in operation from a "normal" to an "excess" condition. For Case 3a, the flow rates were 92 and 384 cm^3/min, corresponding to 1.2/2.0 stoichiometry for the 0.7 V initial condition (i.e., 0.54 A/cm^2) and a stoichiometry of 1.0/1.7 for $t = \infty$ (i.e., 0.5 V and 0.63 A/cm^2). This corresponds to a change in the fuel stoichiometry from a "normal" to a "starved" condition. Note that for fixed voltage a single cell can never be completely "starved" but we use this as a description. Prior to changing the cell voltage, we waited 30 min to ensure a steady-state value of the current and to ensure a well humidified membrane at the voltage. We replicated the experiment at least twice and the data presented here demonstrates reproducibility of the transient responses as discussed below.

All the data reported here were obtained with PRIMEA® Series 5510 MEA (0.4 mg/cm^2 Pt loading, 25 μm nominal membrane thickness, W.L. Gore & Associates, Inc., Elkton, Maryland, USA). The original active electrode area was 25 cm^2, but sub-gaskets for both anode and cathode sides reduced the area to 20 cm^2. The gas diffusion media (GDM) used for both anode and cathode were 16 mils (0.41×10^{-3} m) CARBEL™ CL. The cell was tightened with 8 V at the torque of 50 lb$_f$-in./bolt. The effect of clamp-torque has been discussed by Lee et al. [9]. The flow fields for both anode and cathode used in this experiment had triple path serpentine channels where the flows were split into three paths at entrance and converged at the end.

High purity hydrogen (99.997%) and industrial grade compressed air were used. The fuel cell test station used to control the electrical load, the fuel supply, and the temperature was manufactured by Fuel Cell Technologies (Los Alamos, NM). A model 6060B (Agilent Technologies) was used for the electronic load bank. Digital mass flow controllers (MKS model) were used to control the flow rates and these were calibrated with a bubble flow meter as discussed in [10]. The inlet gases were bubbled through the humidity bottles and from the temperature of those bottles a correlation was used to determine the humidity of inlet fuel gas [10].

The operation of a laboratory scale PEMFC involves inlet gas and water vapor diffusing from flow channels through the GDM to electrode, where the electrochemical reaction takes place. The non-reacted gas and water vapor exit the cell and pass through the back-pressure regulator to a vent. The back-pressure of both anode and cathode sides was 101 kPa. The fuel cell was operated at the temperature of 70 °C and the anode and cathode dew point temperatures were 80 and 70 °C, respectively. These dew point temperatures were calculated from calibration data as discussed in [10].

The experiment was conducted in two parts. First, we measured the polarization behavior of the PEMFC at fixed stoichiometry and those familiar with these experiments will recognize this indicates that fixed the flow rates were varied according to the measured current. These polarization data were obtained between a voltage of 0.45 V and the open circuit voltage in randomized steps of 0.05 V. The flow rates were manually changed according to the current in an

[1] We defined the standard condition as 298 K and 101 kPa.

Table 1
Flow rates, stoichiometries, and voltage change rates for experiments

	Flow rates, A/C (cm^3/min)	Stoichiometry (A/C)		Current density (A/cm^2)		Approximate linear cell voltage change rate (V/s)	Voltage time constant, δ (s)	Overshoot/undershoot(A/cm^2)
		$t = 0$	$t = \infty$	$t = 0$	$t = \infty$			
Case 1, 0.7–0.5 V (excess to normal)								
1a	249/1040	2.9/4.8	1.2/2.0	0.62	1.48	0.17	0.6	N/A
1b	501/1040	5.8/4.8	2.4/2.0	0.62	1.48	0.17	0.6	N/A
1c	301/1260	3.5/8.7	1.2/3.0	0.62	1.80	0.17	0.8	N/A
Case 2, 0.5–0.7 V (normal to excess)								
2a	249/1040	1.2/2.0	2.9/4.8	1.48	0.62	0.17	0.4	N/A
2b	501/1040	2.4/2.0	5.8/4.8	1.48	0.62	0.17	0.4	N/A
2c	301/1260	1.2/3.0	3.5/8.7	1.80	0.62	0.17	0.5	N/A
Case 3, 0.7–0.5 V (normal to starved)								
3a	92/384	1.2/2.0	1.0/1.7	0.54	0.58	0.22	0.4	0.95
3b	185/385	2.4/2.0	1.5/1.2	0.57	0.90	0.22	0.5	0.95
3c	96/600	1.2/3.0	1.0/2.7	0.58	0.58	0.22	0.6	1.15
Case 4, 0.5–0.7 V (starved to normal)								
4a	92/384	1.0/1.7	1.2/2.0	0.58	0.54	0.22	0.2	0.39
4b	185/385	1.5/1.2	2.4/2.0	0.90	0.57	0.22	0.2	N/A
4c	96/600	1.0/2.7	1.2/3.0	0.58	0.58	0.22	0.2	0.35

iterative manner to maintain the fixed stoichiometry. The data (Fig. 1) were obtained at three normal stoichiometric sets: a (standard), b (anode-rich), and c (cathode-rich), corresponding to anode/cathode stoichiometries of 1.2/2.0, 2.4/2.0, and 1.2/3.0, respectively. That is, for example, a stoichiometry of 1.2/2.0 corresponds to flow rates that were 1.2 times greater than required (by the measured current) for hydrogen and 2.0 greater than that required on the cathode for air.

The second part of this experiment measured the transient behavior of the PEM fuel cell. A two channel digital oscilloscope (TDS 210, Tektronix Inc.) was used to record simultaneously both the current response and the voltage forcing function. The current was measured using a "hall effect current sensor" so that it would be converted into voltage signals. Fig. 2 shows a schematic diagram of the experimental setup. The current was converted into voltage signal and then recorded at the first channel (CH-1) of the oscilloscope. The cell potential was measured directly from the fuel cell and recorded at the second channel (CH-2) of the oscilloscope. The cell voltage was changed after a steady-state current was achieved at the initial voltage. These signals were recorded in the oscilloscope from 10 s before the triggering point, at $t = 0$, until 40 s after the triggering point.

We focused the transient experiment on voltages changes either to or from 0.7 and 0.5 V. The test station, computer interface, and electronic load bank limited the rates of voltage change to about 0.2 V/s. Variation in this change was

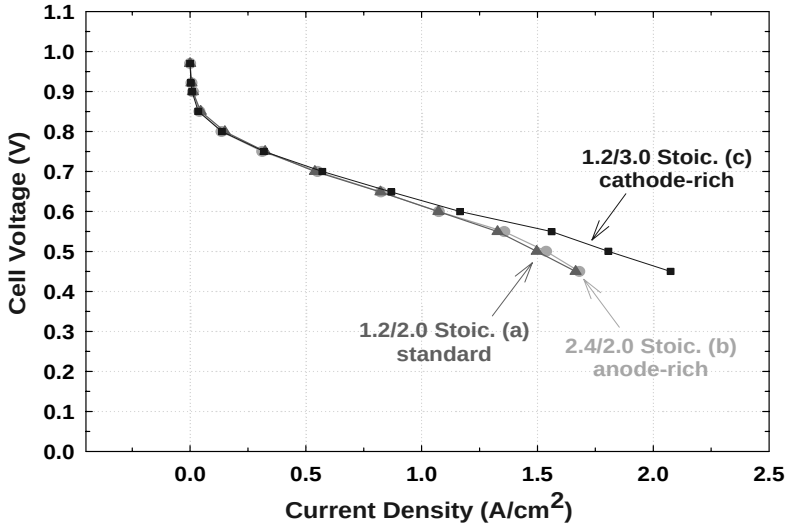

Fig. 1. Steady-state polarization curves for various stoichiometric flows of the anode/cathode: (▲) 1.2/2.0, (●) 2.4/2.0, and (■) 1.2/3.0.

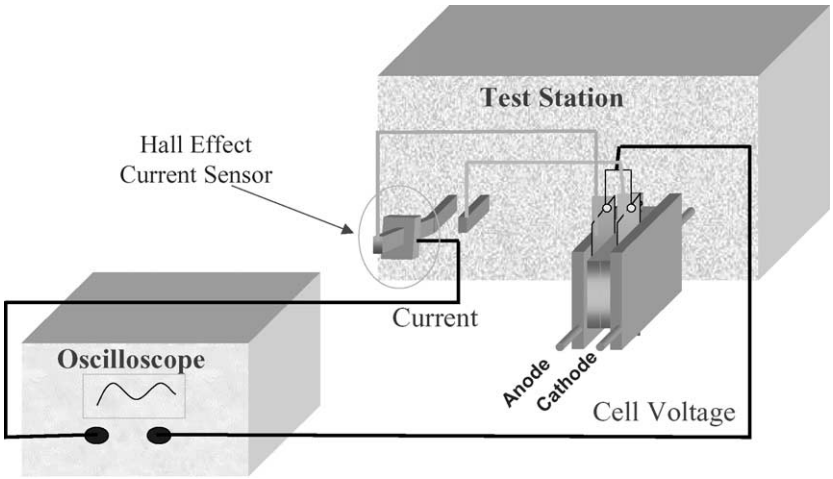

Fig. 2. Schematic diagram of oscilloscope and fuel cell for transient experiments.

±0.05 V/s. The change rates were not linear but rather can be approximated by a first-order system. That is, for Case 1a in Table 1. The cell voltage change rate for this case is approximately 0.17 V/s based on a linear estimate between 0.7 V at $t = 0$ s and 0.5 V at $t = 1.18$ s. Note, however, that the change is not linear but best described as a first-order change:

$$V(t) = V(t = 0) + \Delta V(1 - e^{-t/\delta}) \quad (1)$$

where δ is a time constant that depends on the load characteristics and thus on total current from the PEMFC. For Case 1a, $V(t = 0) = 0.7$ V and $\Delta V = -0.2$ V and for Case 2a $V(t = 0) = 0.5$ V and $\Delta V = +0.2$ V. The time constant, δ, is sown in Table 1. Also for Cases 3 and 4 as shown in Table 1, the linear voltage change rate was approximately 0.22 V/s and thus δ, $V(t) = 0$, and ΔV follow from Table 1.

3. Results and discussions

Fig. 3 shows a voltage–current cycle for a normal-to-excess-to-normal experiment of Cases 1a and 2a. Note that we performed Case 1a followed by Case 2a four times over a period of approximately 4.1 h. Fig. 4 shows the second and third cycles of Fig. 3 and by expanding the time scale for Case 1a it allows comparison of the data obtained at 75 and 135 min. There is some noise in the voltage data corresponding to the ±5 mV accuracy of the load but, in general, the experimental data were reproducible. The response for Case 1a can be described as a first-order (FO) system and one does not observe any overshoot in the current density. That is, the value of 1.16 A/cm^2 occurs at the time constant, τ, of 0.2 s corresponds to 63.2% of the final value of the current density difference between final and initial values. That is, the current density value for this case is

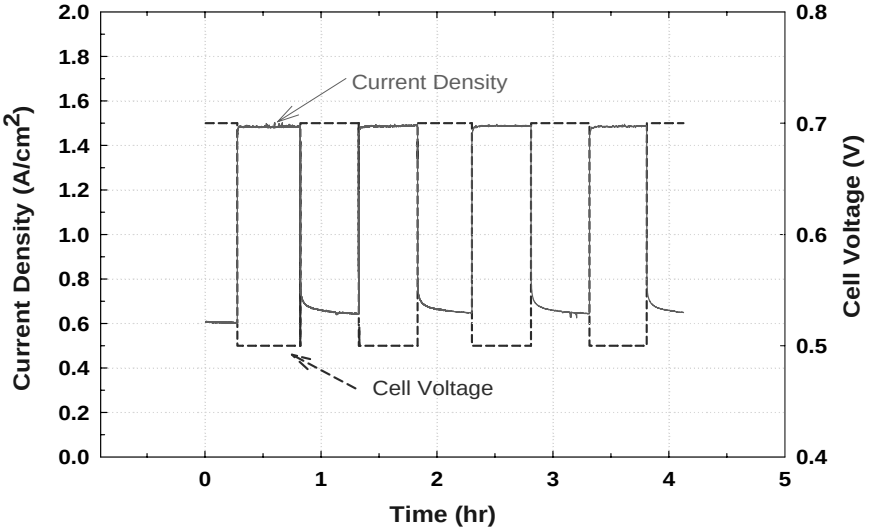

Fig. 3. Overall view of voltage change and current density response for Cases 1a and 2a.

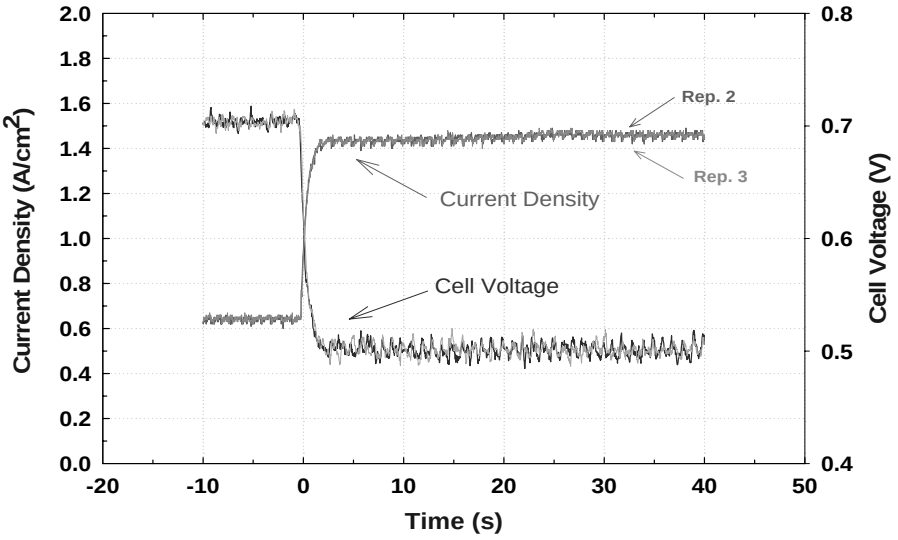

Fig. 4. Case 1a (expanded view with oscilloscope), flow rates: 249/1040 cm^3/min. The cell voltage changes from 0.7 to 0.5 V. Stoichiometry change: 2.9/4.8–1.2/2.0.

$$i(t=\tau) = i(t=0) + 0.632(i(t=\infty) - i(t=0)) \quad (2)$$

where $i(t=0)$ and $i(t=\infty)$ are at initial and final current density, respectively. The transfer function of this FO response system to the voltage change can be written as Laplace domain [11]:

$$i(s) = \frac{K_1}{\tau s + 1} V(s) \quad (3)$$

and by taking the inverse Laplace transform, one can obtain the time domain equation for a step change in V(s):

$$i(t) = i(t=0) + K_1(1 - e^{-t/\tau})(V(t) - V(t=0)) \quad (4)$$

The gain, K_1, is shown in Table 2 to be negative because the forcing function $\Delta V = V(t) - V(t=0)$ is negative (i.e., 0.5–0.7 V). Note that most FO analyses use a step function but that we used (Eq. (1)) for $V(t)$ from the experiments to obtain the value of K_1 with MATLAB® Simulink® as described in [12]. As discussed below the response of current density with a cell voltage change depends mainly on the time constant for the case where the stoichiometry is in excess. The quality of the fit of equation to the data is also discussed below.

Fig. 5 shows the expanded time scale response for Case 2a, a change from 0.5 to 0.7 V at the same flow rates as Case

Table 2
Observations and dependent variables analysis parameters

	Type of response	Gain (A/cm^2 V)		Time constant, τ (s)	FO lead time constant, β (s)	Damping factor, ξ	R^2
		K_1	K_2				
Case 1, 0.7–0.5 V (excess to normal)							
1a	FO	−4.4		0.2			0.9970
1b	FO	−4.4		0.2			0.9970
1c	FO	−5.9		0.2			0.9983
Case 2, 0.5–0.7 V (normal to excess)							
2a	FO	−3.6		0.6			0.9941
2b	FO	−3.6		0.6			0.9941
2c	FO	−5.1		0.6			0.9931
Case 3, 0.7–0.5 V (normal to starved)							
3a	SO L/L	2.4	−2.4	1.5		0.4	0.9643
3b	FO	−1.9		0.02			0.9956
3c	SO L/L	2.8	−2.8	1.1		0.4	0.9472
Case 4, 0.5–0.7 V (starved to normal)							
4a	FO L/L	−0.1		2.0	19		0.9715
4b	FO	−1.4		0.4			0.9816
4c	FO L/L	−0.1		2.0	30		0.9762

The types of responses are abbreviated: FO, first-order system response; FO L/L, first-order lead/lag system response; SO L/L, second-order lead/lag system response (two gains, K_1 and K_2).

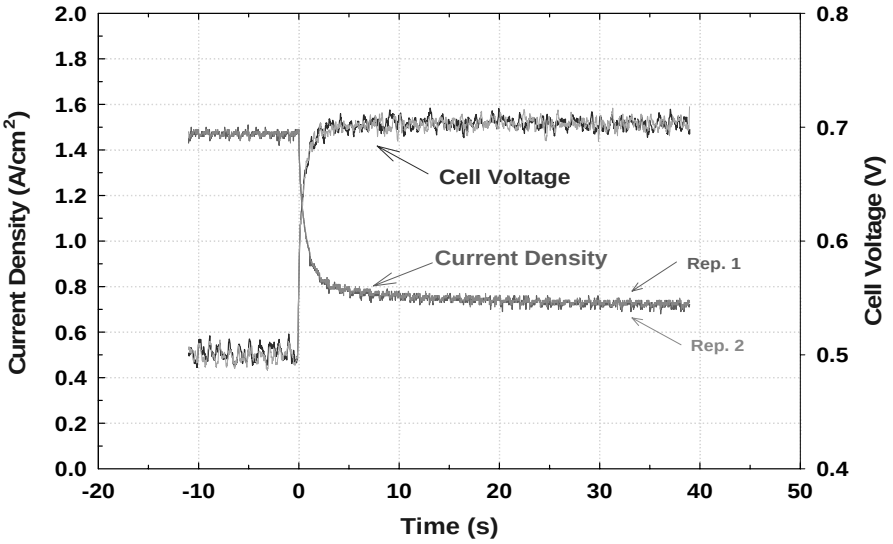

Fig. 5. Case 2a (expanded view with oscilloscope), flow rates: 249/1040 cm^3/min. The cell voltage changes from 0.5 to 0.7 V. Stoichiometry change: 1.2/2.0–2.9/4.8.

1a. Thus, we observed a change from normal stoichiometry to excess (from 1.2/2.0 to 2.9/4.8 stoichiometry). The reproducibility is shown to be good by rescaling the time axis for the data starting at 45 and 105 min and plotting Rep. 1 and Rep. 2 data from Fig. 3. As the cell voltage increases, the current density decreases and this response is also a FO system with the time constant corresponding to about 0.6 s. Note that this FO model and parameters corresponds to the short time response until 0.8 A/cm^2 and that there is a gradual decrease in the current during the next 30 min until the value 0.62 A/cm^2 is obtained at 0.7 V. This current density change for 30 min after a cell voltage change to 0.7 V is reproducible as shown in Fig. 3 and it is typical for this MEA when there are transients at "excess" conditions. The experiments reported here do not yield information on the cause of this long-term decrease. No undershoot behavior is observed for this case. Case 2a can be described by Eqs. (3) and (4) with the parameters of Table 2. For Case 2a the cell voltage change is a positive value and thus the current density decreases so that the gain, K_1, has negative value. Again the comparison of the FO model and the data is discussed after the data for the other cases are presented.

Fig. 6 shows the voltage and current density changes for Cases 3a and 4a. These results were obtained over 2.0 h. The current was unstable (non-periodic oscillations were observed) at the cell voltage of 0.5 V because the hydrogen flow approaches starved conditions. This stoichiometry was estimated based on the average current density at 0.5 V. At a stoichiometry of 1.0 the flow of hydrogen out of the fuel cell will approach zero because all of the

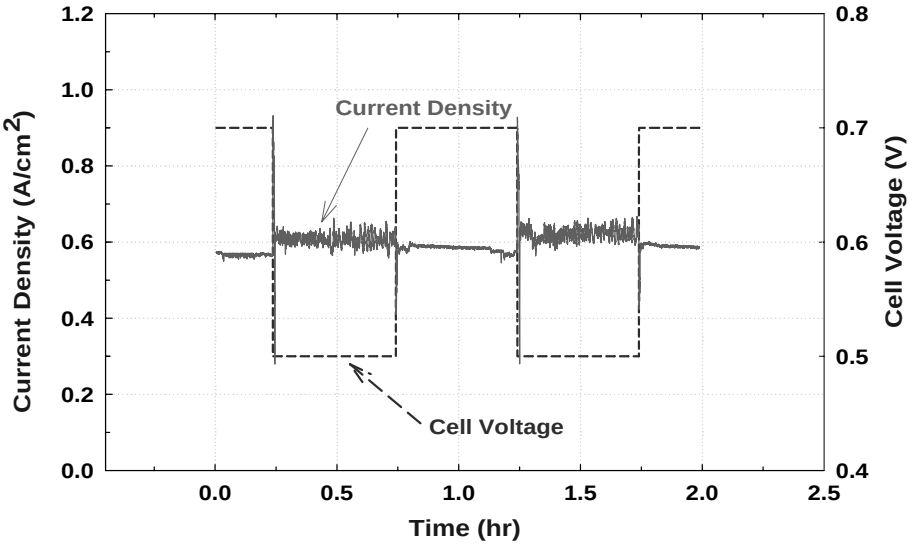

Fig. 6. Overall view of voltage change and current density response for Cases 3a and 4a.

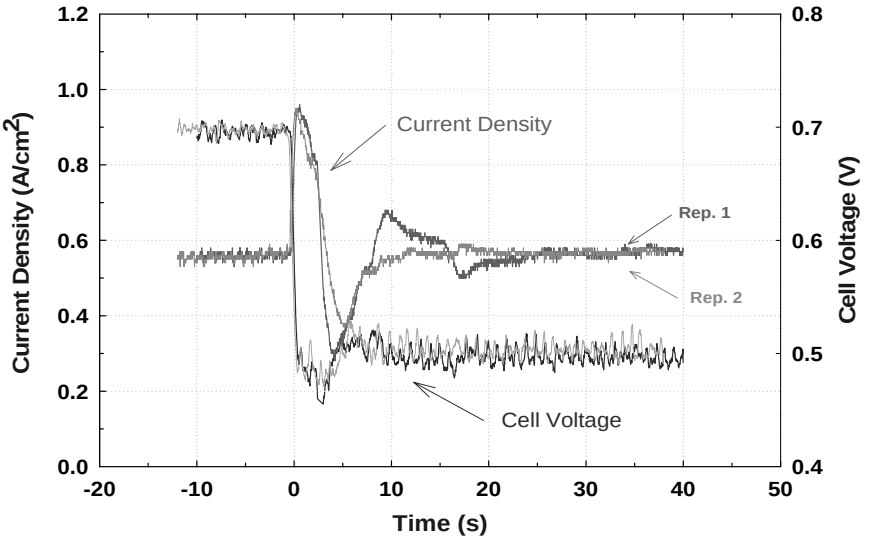

Fig. 7. Case 3a (expanded view with oscilloscope), flow rates: 92/384 cm^3/min. The cell voltage changes from 0.7 to 0.5 V. Stoichiometry change: 1.2/2.0–1.0/1.7.

hydrogen into the cell will be reacted before reaching the end of the flow channel. This is consistence with our numerical predictions [6,7] that indicate for these conditions that all the hydrogen is consumed before reaching the end of the flow channel and that not all the reaction area is utilized.

Fig. 7 expands the scale of Fig. 6 for Case 3a. The stoichiometry changes from a normal (1.2/2.0) to a starved (1.0/1.7) condition (see Table 1) and overshoot behavior is observed here. That is, as the voltage decreases from 0.7 to 0.5 V, the current density increases from 0.54 A/cm^2, at 0.7 V, to about 0.95 A/cm^2 after 0.22 s. This maximum is obtained after the cell voltage reaches 0.5 V and after this maximum, the current density decreases to about 0.38 A/cm^2 for Rep. 1 at 5.5 s and about 0.30 A/cm^2 for Rep. 2 at about 4.5 s. Then at about $t = 10$ s the current density has increased from 0.38 to 0.58 A/cm^2 for Rep. 1. Rep. 2 shows a slightly different behavior where the current density increases from 0.30 A/cm^2 to an apparent second overshoot of 0.68 A/cm^2 at about $t = 10$ s. Typically, we could not confirm that this apparent second overshoot was different from noise but this second overshoot, shown in Fig. 7, corresponds to the maximum value we observed over many replicates. Fig. 7 also shows second undershoot behavior at about $t = 17$ s which again was the extreme that we observed over many replicates. Note that there is some undershoot with the cell voltage in the first 3 s but that this undershoot was only slightly responsible for the width of the overshoot current peak as determined by other experiments.

We now explain the overshoot behavior: Since the electrochemical reaction is greater at 0.5 than at 0.7 V and because the potential of the electrodes follows the cell voltage without any appreciable time lag, the local reaction (i.e., current) uses the excess hydrogen and oxygen without limitation. (The time constants for limitations are discussed below.) This unlimited use continues until 0.95 A/cm^2 (based on 20 cm^2 of MEA area). The current density starts to decrease at 0.22 s because all of the "excess" hydrogen in the GDM and flow channels is consumed. Note that hydrogen is still flowing into the cell but that the distribution of current is highly non-uniform at 0.22 s and becomes more uniform as discussed in [7]. Note also that the overshoot is greater than the 20% that would be expected based on the average stoichiometry. One might be concerned that the MEA hydration may also limit reaction but our experience and measurements indicate that dehydration occurs at a slower time scale than the response shown in Fig. 7 for this MEA.

The undershoot behavior for Case 3a can be explained by considering the current distribution. That is, we hypothesize that the overshoot behavior results in a highly non-uniform current distribution so that the consumption of hydrogen allows for a significant portion of the PEMFC on the hydrogen side to contain ambient air. Ambient air flows into the hydrogen side to equilibrate the atmospheric pressure much like a spring in a spring-dashpot. We label this a "vacuum" effect. This description requires the highly non-uniform current distribution at the peak current density to become more uniform after 10 s as the current density decreases from the peak and it requires time to expel the ambient air and use all of the electrode area. The time between the crossing under the final current density values and the return to the final current density is approximately 9 s for Rep. 1 and 7 s for Rep. 2. The Case 3a can be described with a second-order lead/lag (SO L/L) current response model as discussed below.

Fig. 8 shows the expanded time scale behavior for Case 4a, a change from 0.5 to 0.7 V at the same flow rates as Case 3a. Thus we observe the behavior as the stoichiometry changes from a starved to normal condition (i.e., stoichiometry:

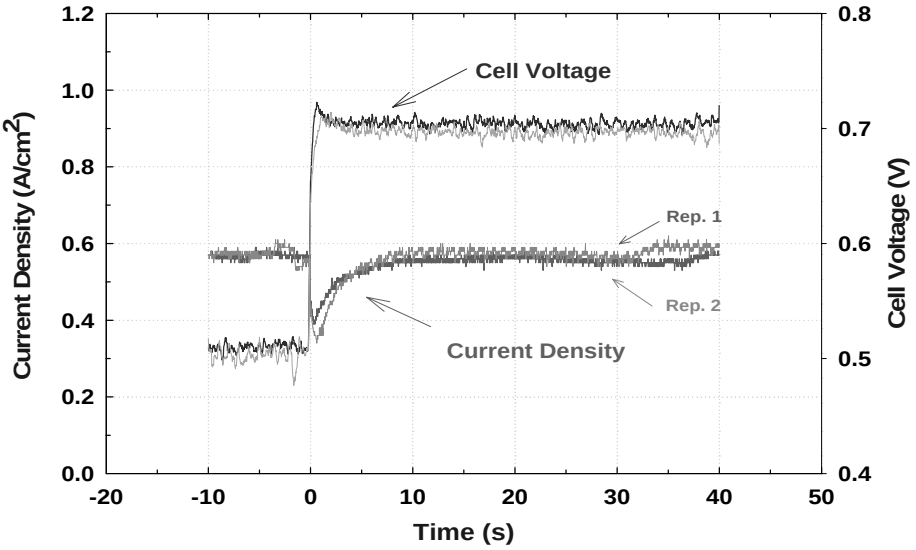

Fig. 8. Case 4a (expanded view with oscilloscope), flow rates: 92/384 cm^3/min. The cell voltage changes from 0.5 to 0.7 V. Stoichiometry change: 1.0/1.7–1.2/2.0.

1.0/1.7 to 1.2/2.0). Here, we observe undershoot behavior in the current density. At the cell voltage of 0.5 V, which is a staved condition, the reaction is probably not uniform and the active area utilization is not complete. However, when the cell voltage is changed to 0.7 V, the electrochemical driving force is less and the current density decreases. The lower current density yields unused fuel. Then, the unused fuel expels the ambient air and the non-utilized reaction area becomes exposed to hydrogen. This re-exposure leads to an increase of current density after about 1 s. The time for the recovery of the undershoot behavior is about 8 s. The responses of Case 4a can be described with a first-order lead/lag (FO L/L) current response model as describe below.

Fig. 9 shows a comparison of the Cases of 1a–1c and it allows analysis of the stoichiometry effect. The three cases, a, b, and c, show similar first-order trends. The response for Cases 1a–1c can be classified as a first-order system because one does not observe an overshoot in the current density when the fuel is excess. The final performance of Case 1c (cathode-rich stoichiometry) shows the highest current density (1.80 A/cm^2) and the initial current densities are equal indicating ohmic limitations at the high initial stoichiometries consistent with Fig. 1 shown in Table 1. Cases 1a and 1b show identical current density responses (0.65 and 1.48 A/cm^2 for initial and final values, respectively). The linear-approximated cell voltage change rates for these three cases are 0.17 V/s and the time constant, δ, for Eq. (1) are close for all three cases. The FO model for the response of the current and a FO response occur for all of these cases because they are not hydrogen-staved condition. Table 2

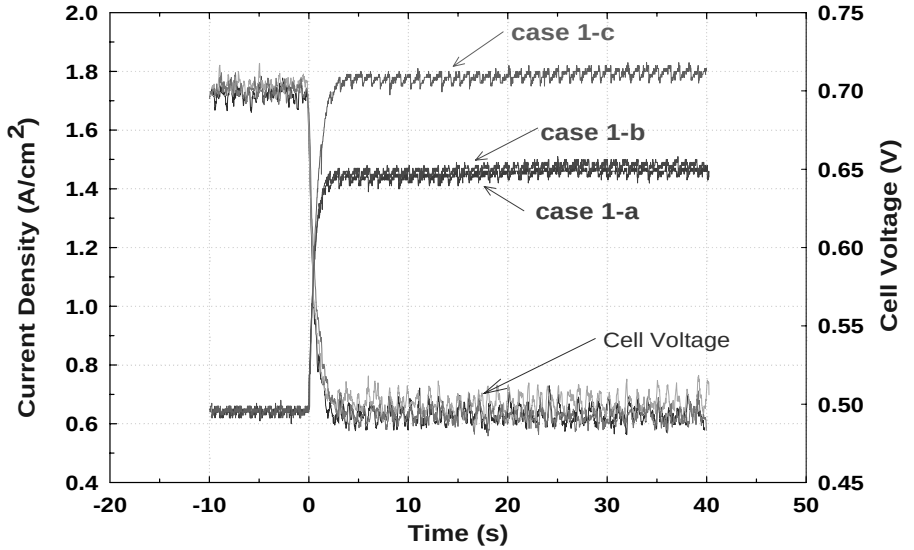

Fig. 9. Comparison of the stoichiometry effect for Cases 1a–1c (excess to normal). See Table 1 for flow rates.

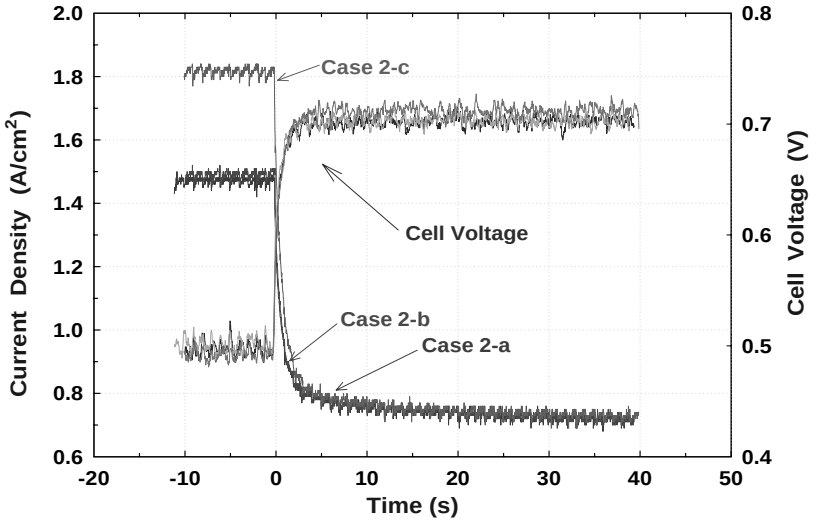

Fig. 10. Comparison of the stoichiometry effect for Cases 2a–2c (normal to excess). See Table 1 for flow rates.

shows that the time constant for each case is the same and that the gain is controlled by the air stoichiometry. This gain could be obtained from steady-state polarization curves such as those shown in Fig. 1 and thus for this configuration of MEA, GDL, gasket, flow field, and membrane water content the FO response can be calculated for design purposes. Future work will quantify the effect of ΔV on τ and K_1 for the excess stoichiometry and other configurations. The lack of a starved condition conditions yields no overshoot behavior. The R^2 shown in Table 2 is one measure of good agreement between the FO model and the data and Ref. [12] contains graphs of these comparisons.

Fig. 10 shows a comparison of Cases 2a–2c. These graphs show similar FO current density responses where the current density decreases when the cell voltage increases. The initial performance of the Case 2c is higher than that of other two cases because the higher cathode stoichiometry air reduces mass transfer limitations. This response system can be characterized with FO response of exponential decay because there is excess fuel. The FO model with the parameters in Table 2 agrees with the experimental data and no undershot behavior is observed. Note that although the time constants are equal, the gain reflects the initial stoichiometry. Note also that these parameters correspond to short time since the final approach to steady-state requires about 30 min (see Fig. 3 and discussion above). This slow long-term decaying is responsible for the difference in K_1 for the respective conditions of Cases 1 and 2. Thus $K_1 = -5.9\,\text{A/cm}^2\,\text{V}$ for Case 1c but $K_1 = -5.1\,\text{A/cm}^2\,\text{V}$ for Case 2c.

Fig. 11a shows a comparison of Cases 3a–3c. These data have more noise due to the "starved" condition but the data are sufficiently reproducible to compare. Case 3b does not show the overshoot/undershoot behavior because there is excess hydrogen. Cases 3a and 3b start at the same current density at 0.7 V (consistence with Fig. 3) but only Case 3b shows a FO responses as indicated in Table 2. Note that the small time constant of 0.02 s indicating the lack of limitations consistent with the lack of mass transfer or membrane hydration issues. Case 3c has the higher air stoichiometry than Case 3a and thus the initial current density for Case 3c is slightly the larger (0.58 versus 0.54 A/cm^2). The responses of Cases 3a and 3c can be classified as a modified second-order response called as second-order lead/lag system (SO L/L). The details of this modification can be found in [12]. The model can be written in the Laplace domain:

$$i(s) = \left(K_2 + \frac{K_1}{\tau^2 s^2 + 2\tau\xi s + 1}\right) V(s) \tag{5}$$

The time domain function for this system can be described by the sum of two current densities, i_1 and i_2, where i_1 corresponds to the current density for all times beyond the time where the current density is a maximum and is described:

$$\tau^2 \frac{d^2 i_1}{dt^2} + 2\xi\tau \frac{di_1}{dt} + i_1 = K(V(t) - V(t=0)) \tag{6a}$$

and where i_2 corresponds to the current density at times before and at the maximum and is described:

$$i_2 = K_2\,[V(t) - V(t=0)] \tag{6b}$$

MATLAB® [13] was used to fit the Eq. (5) to the data and obtain the parameters. The parameters, steady-state gains, K_1 and K_2, the time constant, τ, and the damping factor, ξ, listed in Table 2. When the cell voltage is decreased to 0.5 V, $\Delta V = -0.2$ V, and the current density increases instantaneously to 0.95 and 1.15 A/cm^2 for Cases 3a and 3c, respectively. We model this instantaneous increase with the gain K_2. The condition of K_2 with ΔV is explored in our next paper [12]. The cell voltage difference, ΔV has negative value in this case, -0.2 V, and K_2 has negative value so that the current density response has positive value. After the maximum current density, all the hydrogen stored in the cell is used and the current density begins to decrease. This

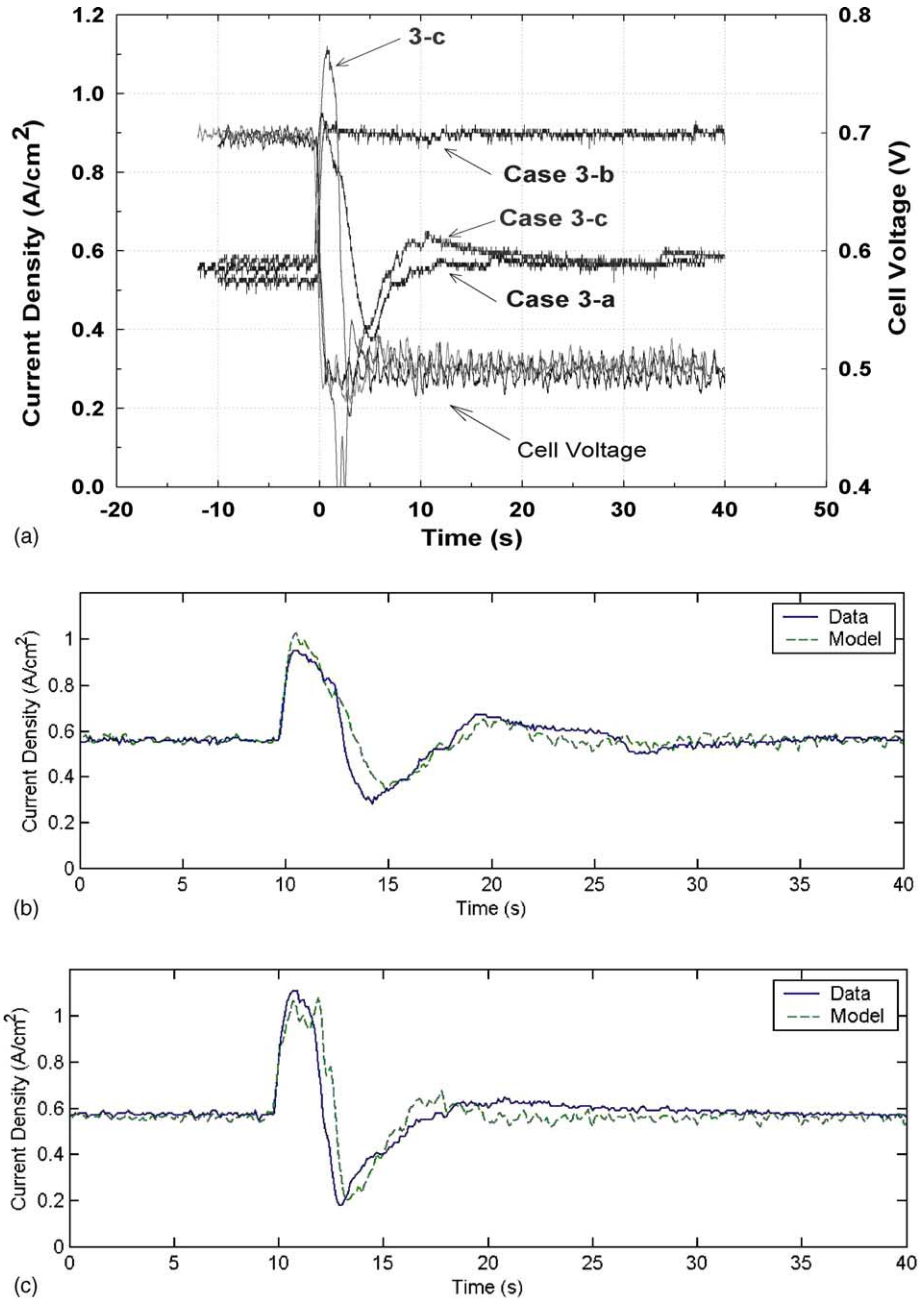

Fig. 11. (a) Comparison of the stoichiometry effect Cases 3a–3c (normal to starved). See Table 1 for flow rates. (b) Fitting of second-order lead/lag response for Case 3a. (c) Fitting of second-order lead/lag response for Case 3c.

decrease is modeled with the second-order part of Eq. (5) and (6). The gain, K_1, has positive value and the ΔV has negative value so that the current begin to decay from the overshoot peak. The time constant can be obtained at 63.2% of this decrease. The current density value at $t = 0$ in that equation in this case is the overshoot peak and that of $t = \infty$. The undershoot behavior is affected by the damping coefficient in the second-order term. The time constants, τ, for Cases 3a and 3c are 1.5 and 1.1 s, respectively. This indicates that the hydrogen consumption is about 1.4 times faster for Case 3c. These parameters could be used for interpolation for any cathode stoichiometry ratio between these two cases. The instantaneous gains, K_2, for Cases 3a and 3c are different based on the difference in overshoot at $t \rightarrow 0$ listed in Table 2. Note that the R^2 values are somewhat smaller for Cases 3a and 3c indicating less agreement between the equation and the data. Fig. 11b and c shows that these comparisons are adequate for a description of the dynamics.

It is interesting to note that the overshoot peak at about 0.95 A/cm^2 for Case 3a is only slightly larger than the value of about 0.90 A/cm^2 observed for Case 3b. The hydrogen is not starved for Case 3b (stoichiometry change from 2.4 to

1.5 for the anode) and thus one might believe that the maximum peak is related to the ohmic drop across the MEA. Thus Case 3b is controlled by oxygen electrode and the IR since there is sufficient hydrogen. Thus Case 3b gives the stable cell performance at 0.5 V, while other two cases show "vacuum" effects and unstable oscillations due to insufficient hydrogen. Also, the undershoot behavior due to the "vacuum" effect after overshoot peak for Case 3c is more significant than that of Case 3a, due to the cathode-rich stoichiometry. The overshoot peak values for Cases 3a and 3c are about 0.95 and 1.15 A/cm^2, respectively. The undershoot behaviors were shown at about $t = 5$ s with a depth of about 0.37 A/cm^2 for Case 3a and at about $t = 2.5$ s and 0.2 A/cm^2 of undershoot value for Case 3c. With similar hydrogen flow rates for Cases 3a and 3c are similar, 92 and 96 cm^3/min, respectively, the hydrogen is consumed faster for Case 3c than for Case 3a because the oxygen is not limited. The electrochemical reaction is more limited by oxygen mass transfer at cell voltage of 0.5 V than 0.7 V. Abundant oxygen for Case 3c results in faster consumption of hydrogen than Case 3a and a larger "vacuum" effect with more ambient air flowing in. Also the second overshoot is observed in Case 3c because we used Rep. 2 of Fig. 7 in Fig. 11a. Again while we cannot completely distinguish, the second peak observed at about $t = 10$ s with the value of about 0.62 A/cm^2 from the noise, one would expect that a second oscillation corresponding to the dashpot system mentioned above is more significant with excess air.

Fig. 12 shows a comparison of the Cases 4a–4c. Case 4b does not show undershoot behavior because the hydrogen flow is not starved. Also, the initial current density, 0.90 A/cm^2, is the same as the final of Case 3b from Fig. 11a. The transient behavior of Case 4b can be classified as a FO response system as explained above. The final current density value in Fig. 12 is about 0.6 A/cm^2 for all cases. However, the undershoot behavior of cathode-rich condition, Case 4c, shows similar behavior as that shown in Case 4a. The undershoot depth for Cases 4a and 4c are about 0.40 and 0.38 A/cm^2 and the recovery times for both cases are also very similar with similar hydrogen flow rates. We explain this similarity as, the cell performance at 0.7 V is more affected by ohmic limitations rather than oxygen mass transfer limitation. Thus the extent of recovering from hydrogen starved conditions is similar for both cases. This similarity strongly supports the hypothesis that the undershoot behavior and recovery rate depends on the hydrogen utilization.

Cases 4a and 4c can be described by a first-order lead/lag (FO L/L) response of current density. The FO L/L system can be written in the Laplace domain as:

$$i(s) = K_1 \frac{\beta s + 1}{\tau s + 1} V(s) \tag{7}$$

The time domain of the transfer function above is

$$i(t) = i(t = 0) + K_1(1 - (1 - \rho)\, e^{-t/\tau})(V(t) - V(t = 0)) \tag{8}$$

where ρ is the lead-to-lag ratio ($=\beta/\tau$) [11,13]. The parameters, lead time constant, β, lag time constant, τ, and steady-state gain, K_1, are listed in Table 2. The gain, K_1, and lead time constant, β, affect the instantaneous undershoot response. The gain represents the difference between initial and final values. Although the initial current density values for Cases 4a and 4c shown in Table 1 are 0.58, the average current density at 0.5 V as mentioned in Fig. 8, for both cases, the model fittings were calculated based on Fig. 12. The undershoot peak is determined by lead-to-lag ratio, ρ and K_1. The ΔV has positive value, 0.2 V, and the gain has negative value so that the current response is negative with the cell voltage change. Then the lag time constant in this

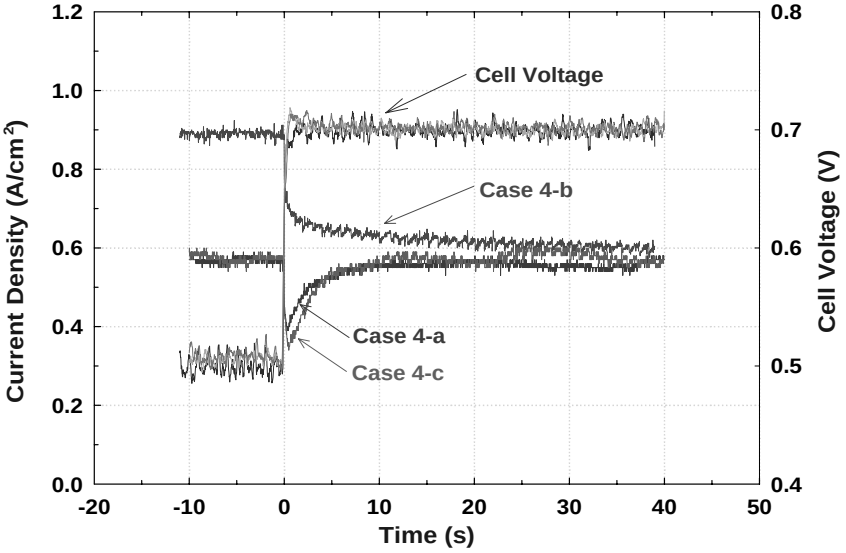

Fig. 12. Comparison of the stoichiometry effect in Cases 4a–4c (starved to normal). See Table 1 for flow rates.

case, τ, affects the current density makeup. The lag time constants, τ, were obtained from experimental data by applying Eq. (2). The initial current density in this case is the undershoot peak value. While the other two cases show first-order lead/lag system, Case 3b shows a modified first-order exponential decay. The hydrogen stoichiometry is changed from 1.5 to 2.4 for Case 3b.

4. Conclusions

Data were presented to show the current density response when the cell voltage was changed rapidly for fixed flow rates. The responses depend on the relative stoichiometry at $t = 0$ and ∞. Overshoot, undershoot, and overshoot/undershoot behavior was observed. For excess stoichiometry, the response was modeled with a FO equation. Thus no overshoot or undershoot behaviors were observed for the excess stoichiometries. For "starved" conditions, pseudo-second-order behavior was observed and classified with lead/lag models. Parameters for these models were presented and the models agree well with the experimental data. Undershoot behaviors were observed when hydrogen stoichiometry is changed from starved to normal condition. The undershoot behavior was explained in terms of a non-uniform hydrogen controlled current distribution. The undershoot peak is affected by the gain, K, and lead-time constant, β, with the cathode stoichiometry. Overshoot behavior was explained in terms of excess hydrogen consumption, non-uniform hydrogen controlled current density, and a sufficient consumption of hydrogen to draw ambient air into the flow field at the exit of the cell. These overshoot peaks are affected by the gain, K_2, for instant, current density increase with cell voltage decrease.

Finally, overshoot followed by undershoot behavior was observed and explained in terms of hydrogen replacing the ambient air as the current density distribution became more uniform. The undershoot following the overshoot peak is affected by second-order gain, K_1, for the steady-state value at $t = \infty$ and damping coefficient, ξ for its magnitude. The cathode stoichiometry affected the time constant, τ, and magnitude of overshoot peak. It supports that the overshoot or undershoot behaviors were mainly dependent on hydrogen utilization.

Acknowledgements

Financial support by the South Carolina State University/University Transportation Center (Grant no. 2000-013), Department of Energy-EPSCoR (Cooperation Agreement DE-FG02-91ER75666), and Office of Naval Research, ONR (Grant no. N00014-98-1-0554) is gratefully acknowledged. The authors gratefully acknowledge that W.L. Gore & Associates, Inc., supplied the MEAs used in this work.

References

[1] J. Hamelin, K. Agbossou, A. Laperriere, F. Laurencelle, T.K. Bose, Int. J. Hydrogen Energy 26 (2001) 625–629.
[2] J.C. Amphlett, E.H. De Oliveria, R.F. Mann, P.R. Roberge, A. Rodrigues, J.P. Salvador, J. Power Sour. 65 (1997) 173–178.
[3] J.C. Amphlett, R.F. Mann, B.A. Peppley, P.R. Roberge, A. Rodrigues, J. Power Sour. 61 (1997) 183–188.
[4] B. Emonts, J. Bøgild Hansen, H. Schmidt, T. Grube, B. Hohlein, R. Peters, A. Tschauder, J. Power Sour. 86 (2000) 228–236.
[5] R. Kötz, S. Müller, M. Bärtschi, B. Schnyder, P. Dietrich, F.N. Büchi, A. Tsukada, G.G. Scherer, P. Rodatz, O. Garcia, P. Barrade, V. Hermann, R. Gallay, in: G. Nazri, et al. (Eds.), Advanced Batteries and Supercapacitors, ECS Proceedings, vol. PV 2001-21, 2001.
[6] S. Shimpalee, W.-k. Lee, J.W. Van Zee, H. Naseri-Neshat, Int. J. Hydrogen Energy, submitted for publication.
[7] S. Shimpalee, W.-k. Lee, J.W. Van Zee, Presented at the 2002 Meeting of the Electrochem. Soc., Paper No. 1136, Philadelphia, PA, May 2002.
[8] M. Ceraolo, C. Miulli, A. Pazio, J. Power Sour. 113 (2003) 131.
[9] W.-k. Lee, C. Ho, J.W. Van Zee, J. Power Sour. 84 (1999) 45.
[10] W.-k. Lee, Ph.D. Dissertation, Department of Chemical Engineering, University of South Carolina, SC, 1999.
[11] B.A. Ogunnaike, W.H. Ray, Process Dynamics, Modeling, and Control, Oxford, 1994, pp. 139–211.
[12] S. Kim, Ph.D. Dissertation, Department of Chemical Engineering, University of South Carolina, SC, 2004.
[13] MATLAB® Simulink®, version 6.5.1. http://www.mathworks.com.